Cai et al. Radiation Oncology (2024) 19:63
https://doi.org/10.1186/s13014-024-02453-2

RESEARCH

Open Access

A non-invasive preoperative prediction model for predicting axillary lymph node metastasis in breast cancer based on a machine learning approach: combining ultrasonographic parameters and breast gamma specific imaging features

Ranze Cai[1†], Li Deng[2†], Hua Zhang[3], Hongwei Zhang[3] and Qian Wu[4*]

Abstract

Background The most common route of breast cancer metastasis is through the mammary lymphatic network. An accurate assessment of the axillary lymph node (ALN) burden before surgery can avoid unnecessary axillary surgery, consequently preventing surgical complications. In this study, we aimed to develop a non-invasive prediction model incorporating breast specific gamma image (BSGI) features and ultrasonographic parameters to assess axillary lymph node status.

Materials and methods Cohorts of breast cancer patients who underwent surgery between 2012 and 2021 were created (The training set included 1104 ultrasound images and 940 BSGI images from 235 patients, the test set included 568 ultrasound images and 296 BSGI images from 99 patients) for the development of the prediction model. six machine learning (ML) methods and recursive feature elimination were trained in the training set to create a strong prediction model. Based on the best-performing model, we created an online calculator that can make a linear predictor in patients easily accessible to clinicians. The receiver operating characteristic (ROC) and calibration curve are used to verify the model performance respectively and evaluate the clinical effectiveness of the model.

Results Six ultrasonographic parameters (transverse diameter of tumour, longitudinal diameter of tumour, lymphatic echogenicity, transverse diameter of lymph nodes, longitudinal diameter of lymph nodes, lymphatic color Doppler flow imaging grade) and one BSGI features (axillary mass status) were selected based on the best-performing model. In the test set, the support vector machines' model showed the best predictive ability (AUC = 0.794, sensitivity = 0.641, specificity = 0.8, PPV = 0.676, NPV = 0.774 and accuracy = 0.737). An online calculator was established for clinicians to

†Ranze Cai and Li Deng contributed equally in this work.

*Correspondence:
Qian Wu
17211210092@fudan.edu.cn

Full list of author information is available at the end of the article

predict patients' risk of ALN metastasis (https://wuqian.shinyapps.io/shinybsgi/). The result in ROC showed the model could benefit from incorporating BSGI feature.

Conclusion This study developed a non-invasive prediction model that incorporates variables using ML method and serves to clinically predict ALN metastasis and help in selection of the appropriate treatment option.

Keywords Breast neoplasms, Axillary lymph node, Machine learning, Ultrasonography, Breast specific gamma image

Background

Breast cancer has become the most prevalent cancer worldwide with an estimated 2.3 million new cases in 2020 [1], the most common route of breast cancer metastasis is through the axillary lymphatic network. Therefore the status of the axillary lymph nodes (ALN) plays an important role in tumour staging, postoperative therapy and tumour prognosis. An accurate assessment of the ALN burden before surgery can avoid unnecessary axillary surgery, consequently preventing surgical complications such as lymphedema, sensory abnormalities, and limitation of upper limb movement [2, 3]. The possibility of exempting axillary surgery in early breast cancer have been widely explored in several clinical trials [4–6]. However, with the limited randomized, multicenter clinical trials and strict inclusion criteria, proper selection of axillary surgeries for patients who fail to meet the criteria has become a priority of many clinicians. Previous studies [7, 8] have attempted to develop models to assess the ALN burden individually to facilitate clinical decision making.

Ultrasonography (US), mammography and magnetic resonance imaging (MRI) are three commonly used imaging modalities for detecting breast cancer, with all techniques relying on the anatomic differences between cancer and normal breast parenchyma [9]. Mammography is the golden standard in cancer screening. However, it remains limited as it only provides information about the anterior axilla when assess the ALN status and its sensitivity is significantly reduced in women with dense breast tissue [10]. MRI shows its superiority in terms of sensitivity and specificity for breast cancer, but some patients are unable to undergo MRI evaluation due to implantable devices, body habitus, renal insufficiency, and claustrophobia. US has the advantage of being convenient, radiation-free, inexpensive and non-invasive. However, in view of the variations between different operators, US has a high false positive rate which limits the clinical application. Therefore, supplementary methods of breast screening must be found. Breast-specific gamma imaging (BSGI) is a recently emerging molecular breast imaging modality that can detect breast cancers at the sub-centimetre level and at various breast tissue densities, with a sensitivity estimate of 90–96% [11, 12]. In BSGI, a radiotracer such as Technetium-99 m Sestamibi is injected into the patient's bloodstream and the breast is visualized using a special camera. The radiotracer uptake is commensurate with blood flow and mitochondrial activity within tumour cells [13], which enables us to diagnose breast cancer by distinguishing the biological behaviour between tumour cells and normal cells. In addition, The BSGI presents an excellent specificity for the diagnosis of ALN metastasis [14]. This prompted us to wonder the possibility of incorporating BSGI, a modality with accuracy comparable to MRI, to improve the accuracy of ALN status prediction. We reviewed the previous literature and found none exploring this possibility yet.

Machine learning (ML) is an emerging tool for cancer prediction and prognosis that is making significant contributions in different cancer fields [15, 16]. It is a learning process capable of providing excellent accuracy through a continuous mechanical learning approach using techniques like decision trees (DTs), artificial neural networks (ANN), and support vector machines (SVM), ultimately developing prediction tools which in some cases outperform traditional statistical modeling.

Thus, the aim of our study was to employ ML-based statistical methods to select variables from non-invasive preoperative modalities, such as BSGI and US, ultimately establish a prediction model to assess the ALN burden, which can guide clinicians for better choice of cancer treatment options for different patients.

Methods

Patients

The clinical data of patients who underwent surgery between January 2012 and May 2021 at Zhongshan Hospital (an affiliate of Fudan University) were collected consecutively and analyzed retrospectively. The inclusion criteria were: 1. Patients has received preoperative BSGI as well as US; 2. The patient has received both breast tumour resection and axillary surgery in our hospital; 3. Postoperative pathologically confirmed diagnosis of breast cancer without neoadjuvant therapy; 4. No history of other tumours. Normal breast and lymph node ultrasounds imagines were excluded. The ethical approval of this study was granted by ethics committee of Zhongshan Hospital. All methods were carried out in accordance with relevant guidelines and regulations. Zhongshan Hospital Ethics Committee waived the need of informed consent from patients since it was a retrospective study. The working flow of our study was showed in Fig. 1.

BSGI and ultrasonographic results

Patients underwent BSGI (Dilon 6800; Dilon Technologies) at high-resolution and a small field-of-view. Imaging was performed 10–15 min after the intravenous administration of 740 MBq Technetium-99 m Sestamibi (GMS Pharmaceutical Co. Ltd) through an antecubital vein contralateral to the suspicious breast side. Craniocaudal (CC) and mediolateral oblique (MLO) images of both breasts were obtained. A low-energy general-purpose collimator was used, with a photopeak focused at 140 keV with a symmetric 10% window. The acquisition time was approximately 6 min per image and a value of 100 000 counts per image was defined as the minimum range.

Two experienced nuclear medicine physicians analyzed the images and were blinded to the patients' clinical information and pathological results. According to the 2010 guidelines of the Breast Imaging Reporting and Data System (BIRADS) of the Society and Nuclear Medicine and Molecular Imaging [17], lesions with homogeneous and small patchy uptake were considered to be negative, lesions with patchy uptake, mild focal uptake

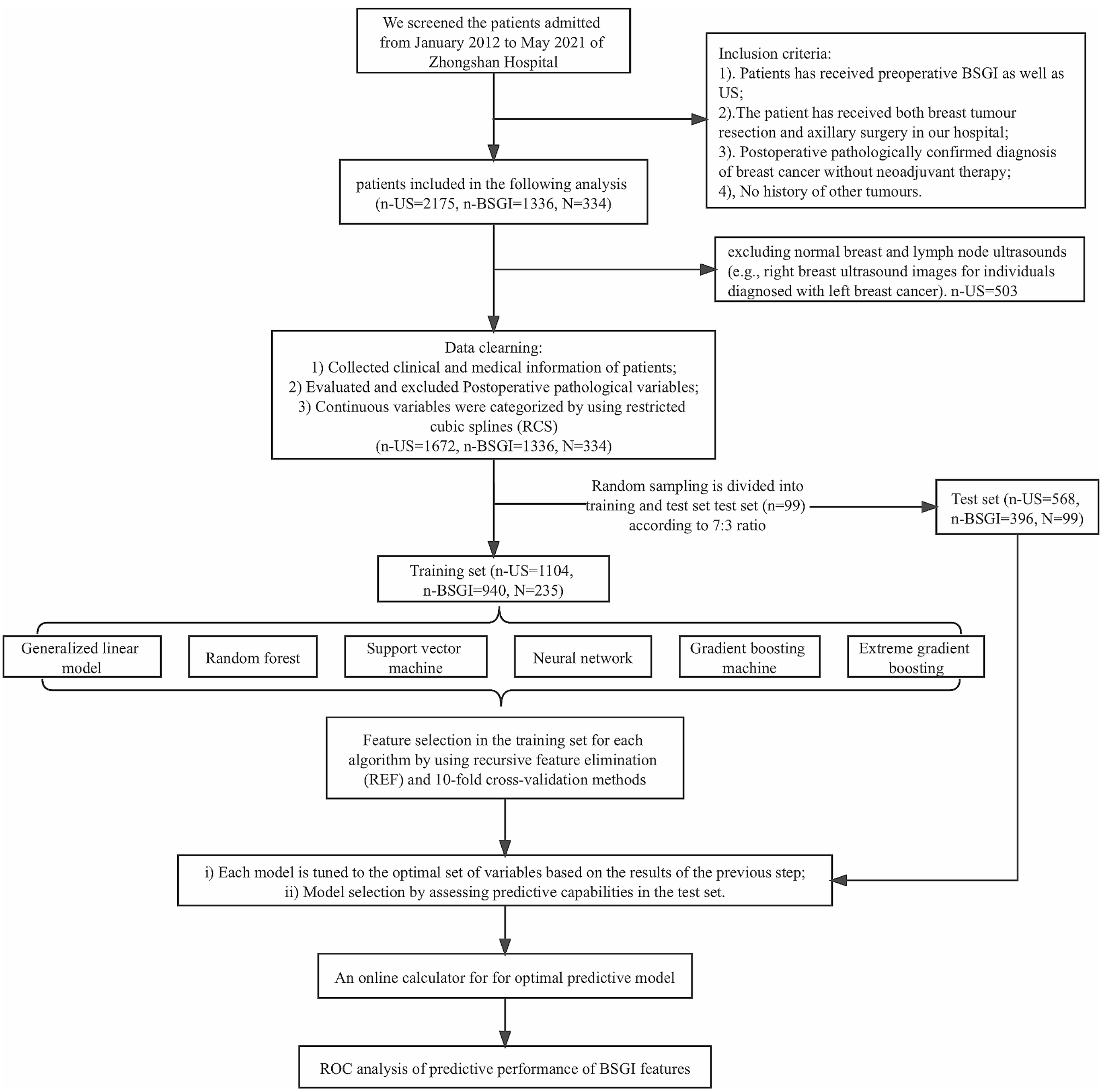

Fig. 1 Working flow of this study

and definite focal uptake were considered to be positive. The tumour-to-normal lesion ratio (TNR) was calculated by dividing the maximal pixel counts of the tumor lesion by that of normal background breast tissue on both CC and MLO view. A positive axillary mass was considered to be patchy, mild focal and definite focal uptake of Technetium-99 m Sestamibi in axilla. An example of BSGI imagines analysis was showed in Fig. 2.

The ultrasonographic images were obtained using an HDI 5000 scanner (Philips Medical Systems) and analyzed by 2 experienced operators. According to Adler's method [18], the degree of blood flow signal within the breast carcinomas and axillary lymph nodes was subjectively classified into 1 of 4 levels: absent (grade 0), minimal (grade 1), moderate (grade 2), or abundant (grade 3). The echogenicity was classified as cystic (no echo), hypoechoic, isoechoic, hyperechoic and mixed echoic. When a mass showed echogenicity minimally less than that of subcutaneous fat, it was defined as hypoechoic. An example of ultrasonographic imagines analysis was showed in Fig. 3.

Data collection

The collected clinical and medical information of patients included the patients' gender, age, breast tumour location, BSGI features (tumour TNR and axillary mass status), postoperative pathological features (estrogen receptor (ER) status, proliferation index (Ki-67), progesterone receptor (PR) status, Her-2 overexpression, lymphovascular invasion (LVI), Scarff-Bloom-Richardson (SBR) grade, T stage, N stage, infiltration depth, histologic type, molecular subtype, and multifocality) and ultrasonographic parameters of tumour and axillary lymph nodes (sizes, echogenicity, margin, lymph node hilum status, color Doppler flow imaging (CDFI) grade, and resistance index (RI)).

Statistical analysis

Clinical and pathological variables associated with the risk of lymph node metastasis were assessed on the basis of their clinical importance and predictors identified in previously published articles [19, 20]. Categorical variables, such as patients' gender, tumor location, axillary mass status (BSGI), tumor echogenicity, tumor margin, tumor CDFI, lymphatic echogenicity, absence of lymph node hilum, lymphatic CDFI, infiltration depth, histologic type, SBR grade, ER status, PR status, Ki-67, Her-2 overexpression, molecular subtype, LVI, multifocality, T stage, and N stage, were reported as integers and proportions. On the other hand, continuous variables, including patients' age, tumor TNR (CC), tumor TNR (MLO), transverse diameter of tumor, longitudinal diameter of tumor, tumor RI, transverse diameter of lymph nodes, and longitudinal diameter of lymph nodes, were

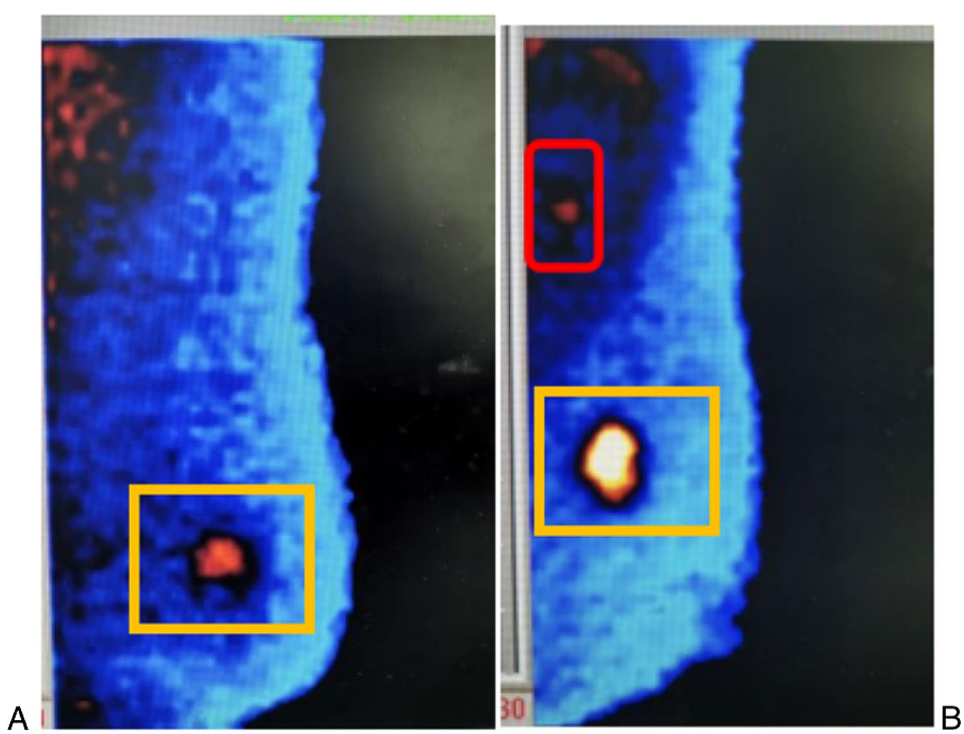

Fig. 2 An example of breast-specific gamma imaging analysis. (**A**) showed a left-sided breast cancer without axillary lymph node metastasis, the yellow rectangle showed the uptake of Technetium-99 m Sestamibi in breast. (**B**) showed a left-sided breast cancer with axillary lymph node metastasis, the red circle showed a positive axillary mass

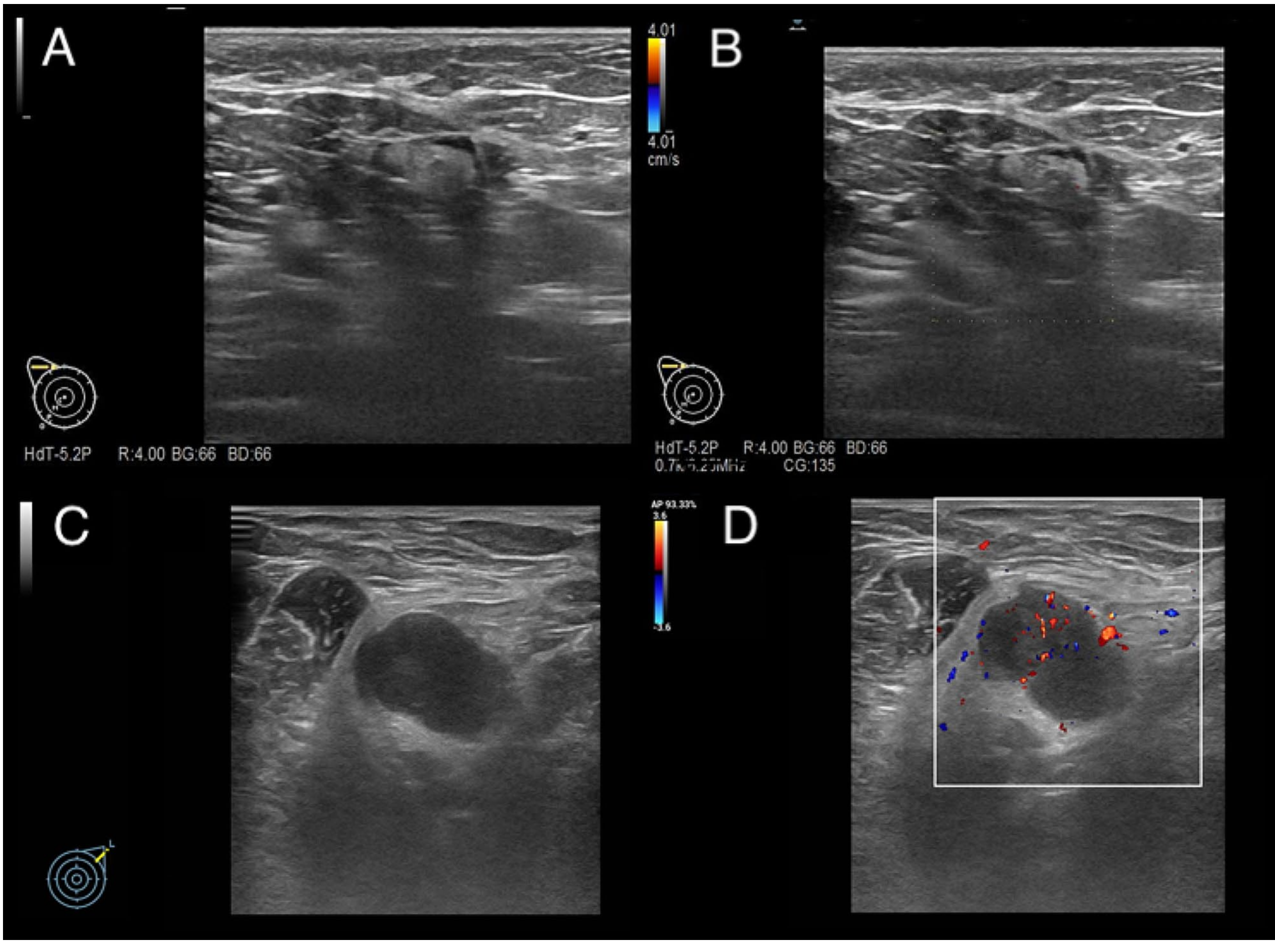

Fig. 3 An example of ultrasonographic lymph node imagines analysis. (**A**) showed an ultrasound image of the right axilla exhibiting no signs of lymph node metastasis. (**B**) showed a color Doppler flow imaging (CDFI) image of the right axilla, indicating the absence of lymph node metastasis. (**C**) showed an ultrasound image of the left axilla showcasing lymph node metastasis, featuring a 24.0*16.0 mm mass identified as a lymph node. (**D**) showed a CDFI ultrasound image of lymph node metastasis in the left axilla, revealing discernible colored blood flow within the affected lymph node

reported as means with standard deviations. The association between clinicopathological characteristics and ALN status was analyzed using X2 test or t-test as appropriate. Collinearity for all explanatory variables were assessed using correlation matrix and plausible interaction terms were also tested. To relax the assumption of a linear relationship between continuous predictors and the risk of ALNs metastasis, continuous variables (such as the patients' age, tumor TNR (CC), tumor TNR (MLO), transverse diameter of tumor, longitudinal diameter of tumor, tumor RI, transverse diameter of lymph nodes, and longitudinal diameter of lymph nodespatient) were converted into categorical variables after valuation using restricted cubic splines (RCS) [21]. Patients were randomly sampling into the training and test sets by ratio 7 : 3. Six machine learning (ML) methods were trained in, including generalized linear model (GLM), random forest (RF), support vector machines (SVM), neural network (NNET), gradient boosting machine (GBM), extreme boosting machine (XGB) [22–24]. To select the strongest predictive variables, recursive feature elimination (REF) was used for each algorithm. To avoid overfitting in training, the best hyper-parameter for ML models was 10-fold cross-validation. Comparison of ML methods performance, the best classification model was select. Based on the best-performing model, we created an online calculator that can make predictor in patients easily accessible to clinicians. Finally, the receiver operating characteristic (ROC) analysis was used to assess the role of BSGI feature in this prediction model [25]. All statistical analyses were determined using the R software (version 3.6.3, http://www.r-project.org). The R packages "caret", "rms", "glmnet", "randomForest", 'nnet', "e1071", "kernlab", "pROC", "gbm", and "xgboost" were used. The "shiny" package was used for web application. We used t-test for continuous variables and chi-square test for classified variables. A two sided $P<0.05$ was considered statistically significant.

Results

Demographic and clinicopathological characteristics

A total of 1672 ultrasound images and 1336 BSGI images from 334 patients were screened between January 2012 to May 2021. Patients were grouped into two groups according to the presence/absence of axillary lymph metastasis. The clinicopathological characteristics between the metastasis and non-metastasis patients were shown in Table 1. The median patient age was 58 years, and 52.1% patients' tumour located on upper-outer quadrant. Patients showed no difference in gender, age, location, tumour echogenicity, tumour margin, tumour CDFI grade, lymph node hilum status, histological type, multifocality, ER, PR, or Her-2 status. However, a higher value of tumour TNR either on CC or MLO view, a positive axillary mass on BSGI, a lower lymphatic echogenicity, a longer transverse or longitudinal diameter of tumour or lymph node, a higher CDFI grade of lymph node, a higher SBR grade, a higher proliferation index (Ki-67), a deeper infiltration, Her-2 positive subtype and the presence of tumour LVI each showed a higher likelihood for ALN metastasis ($P<0.05$).

Prediction model and factors selection

Patients were randomly divided into the training and test groups (group ratio 7 : 3). The training set comprised 1672 ultrasound images and 940 BSGI images sourced from 235 patients. Conversely, the test set consisted of 568 ultrasound images and 396 BSGI images collected from 99 patients. All explanatory variables were turned into categorical form and the cutoffs of continuous variables after RCS processing. All pathological characteristics were excluded since we intended to build a non-invasive model. No statistical difference of variables between training set and test set was found in Table S1. We use six ML methods and combine them with REF to select the optimal combination of variables within each algorithm (Figure S1). The optimal sets of variables for each algorithm in the training set were selected, these variables sets were then passed into each ML method to tune and validated the model in the test set. In Fig. 4A; Table 2, the model of SVM showed best predictive ability in the test set (AUC=0.794, sensitivity=0.641, specificity=0.8, PPV=0.676, NPV=0.774 and accuracy=0.737).

Relative importance of variables in machine learning algorithms

The relative weights of each optimal variables set in each model were shown in Fig. 4B-G. The best parameters of each model for their optimal variables were shown in Table S2.

Although obvious differences were shown in the importance of variables among those ML algorithms, factors including lymphatic CDFI grade, lymphatic echogenicity and BSGI axillary mass status rank top three without fail. However, if only these three variables were selected it would affect the classification results of the ML algorithms. The importance of high-ranking variables in the SVM model is arranged as follows in a descending order: lymphatic CDFI grade, lymphatic echogenicity, longitudinal diameter of lymph nodes, axillary mass status, transverse diameter of lymph nodes, longitudinal diameter of tumour, transverse diameter of tumour.

Web-based calculator

An online calculator based on the best-performing model was established for clinicians to predict patients' risk of ALN metastasis by simply inputing preoperative clinicopathological variables (https://wuqian.shinyapps.io/shinybsgi/) (Fig. 5).

Clinical application evaluation of BSGI

In Fig. 6, a ROC analysis showed that using the final SVM model with BSGI features provided additional benefit from only ultrasonographic features. Thus, We believed the inclusion of BSGI was important to improve preoperative prediction of ALN metastasis in breast cancer patients, especially when lymph node metastases cannot be identified by ultrasonography. This can facilitate early clinical intervention and thus support personalized postoperative cancer rehabilitation.

Discussion

The shift toward less invasive local treatment for axillary sugery is inevitable with the increased use of systemic and radiation therapy. The NSABP b-32 [4] trial found that sentinel lymph nodes biopsy (SLNB) alone without further ALN dissection (ALND) is an appropriate therapy for the targeted patients and has become a routine surgical procedure. Although the incidence of complications after SLNB is relatively low compared to ALND [26], given that dissection of the mammary lymphatic network is unavoidable during SLNB, patients undergoing SLNB may similarity experience subsequent complications such as limited range of motion, lymphoedema, pain, and sensory defects [2, 3]. It prompted us to ponder whether we could exempt axillary surgery for patients with a particularly small probability of metastasis, whether we could develop a completely non-invasive model to predict the probability of ALN metastasis to improve the patients' quality of life.

In this study, we attempted for the first time to combine BSGI features and ultrasonographic parameters to predict ALN metastasis, six different ML methods were analysed and compared to derive optimal solutions for the combination of variables, and the SVM model was found to have the best performance. Six ultrasonographic parameters (transverse diameter of tumour, longitudinal

Table 1 Differences of clinicopathological characteristics between the patients with and without axillary lymph metastasis

	Metastasis ($n=131$)	Non-Metastasis ($n=203$)	All ($n=334$)	*P*value
Gender				
male	1 (0.8%)	2 (1.0%)	3 (0.9%)	
female	130 (99.2%)	201 (99.0%)	331 (99.1%)	1
Age	56.8 (11.9)	58.5 (11.5)	57.8 (11.7)	0.182
Tumour location				
UOQ	68 (51.9%)	106 (52.2%)	174 (52.1%)	
LOQ	27 (20.6%)	34 (16.7%)	61 (18.3%)	
UIQ	23 (17.6%)	42 (20.7%)	65 (19.5%)	
LIQ	12 (9.2%)	14 (6.9%)	26 (7.8%)	
central	1 (0.7%)	5 (3.5%)	6(2.3%)	0.410
BSGI features				
Number of BSGI images	524 (39.2%)	812 (60.8%)	1336 (100%)	
Tumour TNR (CC)	3 (1.3)	2.7 (1.3)	2.8 (1.3)	0.007
Tumour TNR (MLO)	2.9 (1.4)	2.5 (1.2)	2.6 (1.3)	0.002
Axillary mass				
negative	73 (55.7%)	180 (88.7%)	253 (75.7%)	
positive	58 (44.3%)	23 (11.3%)	81 (24.3%)	< 0.001
Ultrasonographic features				
Number of ultrasound images	654 (39.1%)	1018 (60.9%)	1672 (100%)	
Tumour echogenicity				
hypoechoic	129 (98.5%)	196 (96.6%)	325 (97.3%)	
isoechoic	1 (0.8%)	0 (0.0%)	1 (0.3%)	
mixed	1 (0.8%)	7 (3.4%)	8 (2.4%)	0.137
Transverse diameter of tumour (mm)	24.1 (10.3)	20.7 (9.8)	22 (10.1)	0.001
longitudinal diameter of tumour (mm)	15.1 (6.4)	13.7 (6.4)	14.2 (6.4)	
Tumour margin				
regular	1 (0.8%)	3 (1.5%)	4 (1.2%)	
irregular	130 (99.2%)	200 (98.5%)	330 (98.8%)	0.943
Tumour CDFI				
no signal (0)	16 (12.2%)	31 (15.3%)	47 (14.1%)	
spot (I)	7 (5.3%)	20 (9.9%)	27 (8.1%)	
linear (II)	64 (48.9%)	89 (43.8%)	153 (45.8%)	
abundant (III)	44 (33.6%)	63 (31.0%)	107 (32.0%)	0.372
Tumour RI	0.7 (0.3)	0.6 (0.3)	0.7 (0.3)	
Lymphatic echogenicity				
cystic	26 (19.8%)	90 (44.3%)	116 (34.7%)	
hyperechoic	26 (19.8%)	83 (40.9%)	109 (32.6%)	
hypoechoic	76 (58.0%)	29 (14.3%)	105 (31.4%)	
isoechoic	2 (1.5%)	1 (0.5%)	3 (0.9%)	
mixed	1 (0.9%)	0 (0.0%)	1 (0.4%)	< 0.001
Transverse diameter of lymph nodes (mm)	13.6 (10)	6.4 (6.2)	9.2 (8.7)	< 0.001
longitudinal diameter of lymph nodes (mm)	8 (6.6)	3.1 (3)	5 (5.3)	< 0.001
Absence of lymph node hilum				
no or not described	126 (96.2%)	201 (99.0%)	327 (97.9%)	
yes	5 (3.8%)	2 (1.0%)	7 (2.1%)	0.17
Lymphatic CDFI				
no signal (0)	62 (47.3%)	187 (92.1%)	249 (74.6%)	
spot (I)	10 (7.6%)	7 (3.4%)	17 (5.1%)	
linear (II)	38 (29.0%)	6 (3.0%)	44 (13.2%)	
abundant (III)	21 (16.0%)	3 (1.5%)	24 (7.2%)	< 0.001
Lymphatic RI	0.1 (0.3)	0 (0)	0 (0.2)	< 0.001
Pathological features				

Table 1 (continued)

	Metastasis (*n* = 131)	Non-Metastasis (*n* = 203)	All (*n* = 334)	*P*value
Infiltration depth				
in situ	0 (0.0%)	13 (6.4%)	311 (93.1%)	
infiltrative	128 (97.7%)	183 (90.1%)	10 (3.0%)	
other	3 (2.3%)	7 (3.4%)	13 (3.9%)	0.01
Histologic type				
ductal	124 (94.7%)	186 (91.6%)	310 (92.8%)	
lobular	4 (3.1%)	6 (3.0%)	10 (3.0%)	
other	3 (2.3%)	11 (5.4%)	14 (4.2%)	0.379
SBR grade				
not described	5 (3.8%)	42 (20.7%)	47 (14.1%)	
I	3 (2.3%)	10 (4.9%)	13 (3.9%)	
II	53 (40.5%)	81 (39.9%)	134 (40.1%)	
III	70 (53.4%)	70 (34.5%)	140 (41.9%)	< 0.001
Estrogen receptor status				
negative	30 (22.9%)	59 (29.1%)	89 (26.6%)	
positive	101 (77.1%)	144 (70.9%)	245 (73.4%)	0.264
Progesterone receptor status				
negative	44 (33.6%)	80 (39.4%)	124 (37.1%)	
positive	87 (66.4%)	123 (60.6%)	210 (62.9%)	0.338
Proliferation index (Ki-67)				
< 14%	17 (13.0%)	51 (25.1%)	68 (20.4%)	
≥ 14%	114 (87.0%)	152 (74.9%)	266 (79.6%)	0.011
Her-2 overexpression				
negative	89 (67.9%)	156 (76.8%)	245 (73.4%)	
positive	42 (32.1%)	47 (23.2%)	89 (26.6%)	0.095
Subtype				
Luminal A	13 (9.9%)	39 (19.2%)	52 (15.6%)	
Luminal B	88 (67.2%)	105 (51.7%)	193 (57.8%)	
Her2 positive	19 (14.5%)	26 (12.8%)	45 (13.5%)	
Triple negative	11 (8.4%)	33 (16.3%)	44 (13.2%)	0.009
lymphovascular invasion				
no	95 (72.5%)	190 (93.6%)	285 (85.3%)	
yes	36 (27.5%)	13 (6.4%)	49 (14.7%)	< 0.001
Multifocality				
no	127 (96.9%)	199 (98.0%)	326 (97.6%)	
yes	4 (3.1%)	4 (2.0%)	8 (2.4%)	0.791
T stage				
Tis	0 (0.0%)	13 (6.4%)	13 (3.9%)	
T1	57 (43.5%)	116 (57.1%)	173 (51.8%)	
T2	68 (51.9%)	68 (33.5%)	136 (40.7%)	
T3	6 (4.6%)	6 (3.0%)	12 (3.6%)	< 0.001
N stage				
N0	0 (0.0%)	203 (100%)	203 (60.8%)	
N1	70 (53.4%)	0 (0%)	70 (21.0%)	
N2	38 (29.0%)	0 (0%)	38 (11.4%)	
N3	23 (17.6%)	0 (0%)	23 (6.8%)	< 0.001

UOQ: Upper-outer quadrant; LOQ: Lower-outer quadrant; UIQ: Upper-inner quadrant; LIQ: Lower-inner quadrant; BSGI: breast specific gamma image; TNR: tumour-to-normal lesion ratio; CC: craniocaudal; MLO: mediolateral oblique; CDFI: color Doppler flow imaging; RI: resistance index; SBR grade: Scarff-Bloom-Richardson grade

Table 2 Predictive performance comparison of different machine learning models in the test set

ML model	Accuracy	Kappa	Sensitivity	Specificity	PPV	NPV	AUC
GLM	0.758	0.453	0.487	0.933	0.826	0.737	0.774
RF	0.778	0.508	0.564	0.917	0.815	0.764	0.78
SVM	0.737	0.445	0.641	0.8	0.676	0.774	**0.794**
NNET	0.768	0.507	0.667	0.833	0.722	0.794	0.768
GBM	0.737	0.435	0.59	0.833	0.697	0.758	0.784
XGB	0.737	0.435	0.59	0.833	0.697	0.758	0.782

ML: machine learning; GLM: generalized linear model; RF: random forest; SVM: support vector machine; NNET: neural network; GBM: gradient boosting machine; XGB: extreme boosting machine; PPV: Positive predictive value; NPV: Negative predictive value; AUC: the area under the ROC curve.

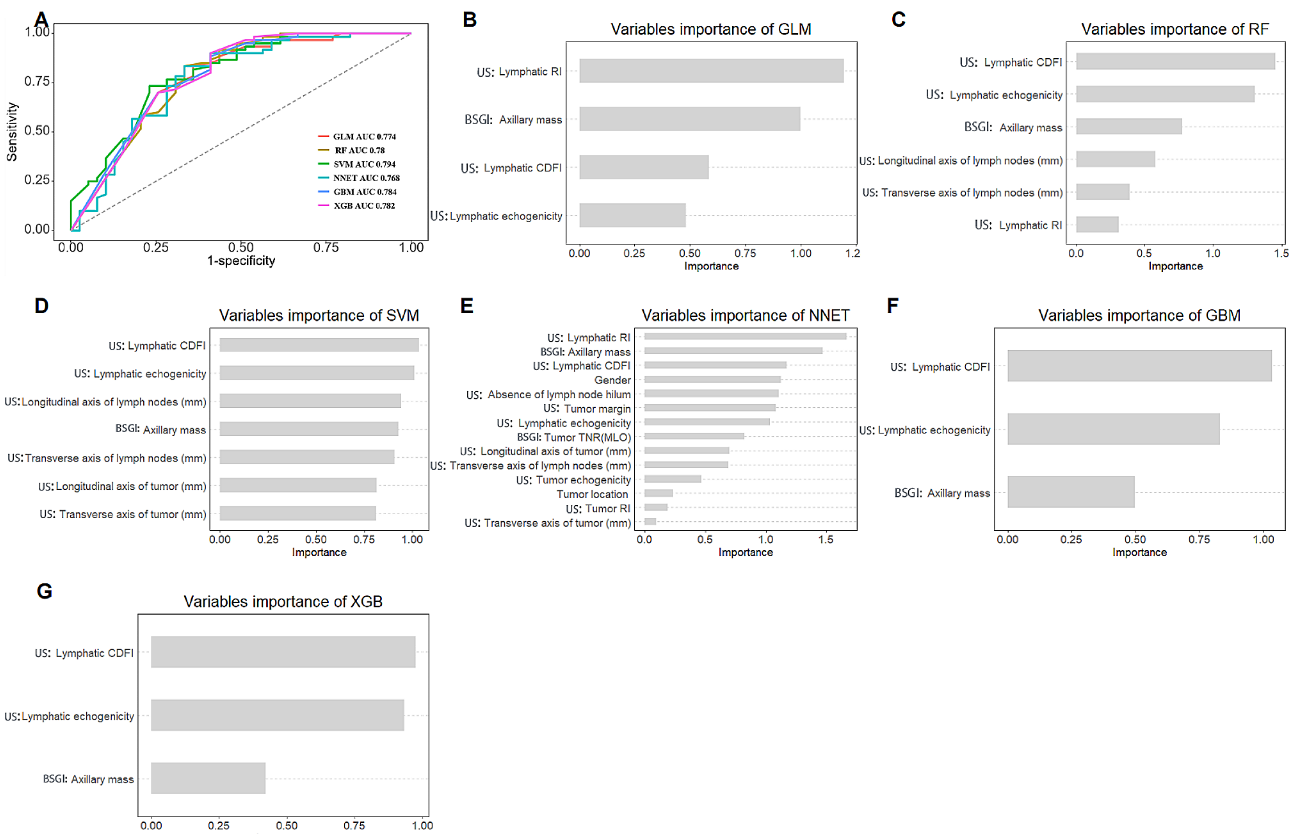

Fig. 4 Model selection. (**A**) The line graph shows the predictive values of each model in test set. (**B-G**) The relative weights of selected variables in each model. GLM: generalized linear model; RF: random forest; SVM: support vector machine; NNET: neural network; GBM: gradient boosting machine; XGB: extreme boosting machine; RI: resistance index; CDFI: the color Doppler flow imaging grade; TNR: tumour-to-normal lesion ratio; MLO: mediolateral oblique; BSGI: breast specific gamma image; US: Ultrasonography

diameter of tumour, lymphatic echogenicity, transverse diameter of lymph nodes, longitudinal diameter of lymph nodes, lymphatic CDFI grade) and one BSGI features (axillary mass status) were eventually incorporated into the final model. The final AUC value obtained for the test set was 0.794, which showed a comparatively high prediction ability. While SVM exhibited the highest AUC values, we observed closely clustered AUC values among the six ML methods, ranging from 0.76 to 0.79. In a study by Zhu et al. [27], six ML methods were applied to predict postoperative central lymph node metastasis in T1-T2 thyroid cancers, yielding AUCs between 0.69 and 0.75. In another study by Wu et al. [28], seven ML methods were used to predict central lymph node metastasis in thyroid cancer, with AUCs ranging from 0.68 to 0.73. Although a slightly larger discrepancy in AUC values exists between these studies compared to ours, it is apparent that the variation in AUC values across all ML methods is not substantial. We attribute this lack of significant difference to the fact that both the training and validation cohorts were sourced from the same institution without external validation, a limitation we'll address in our forthcoming sections.

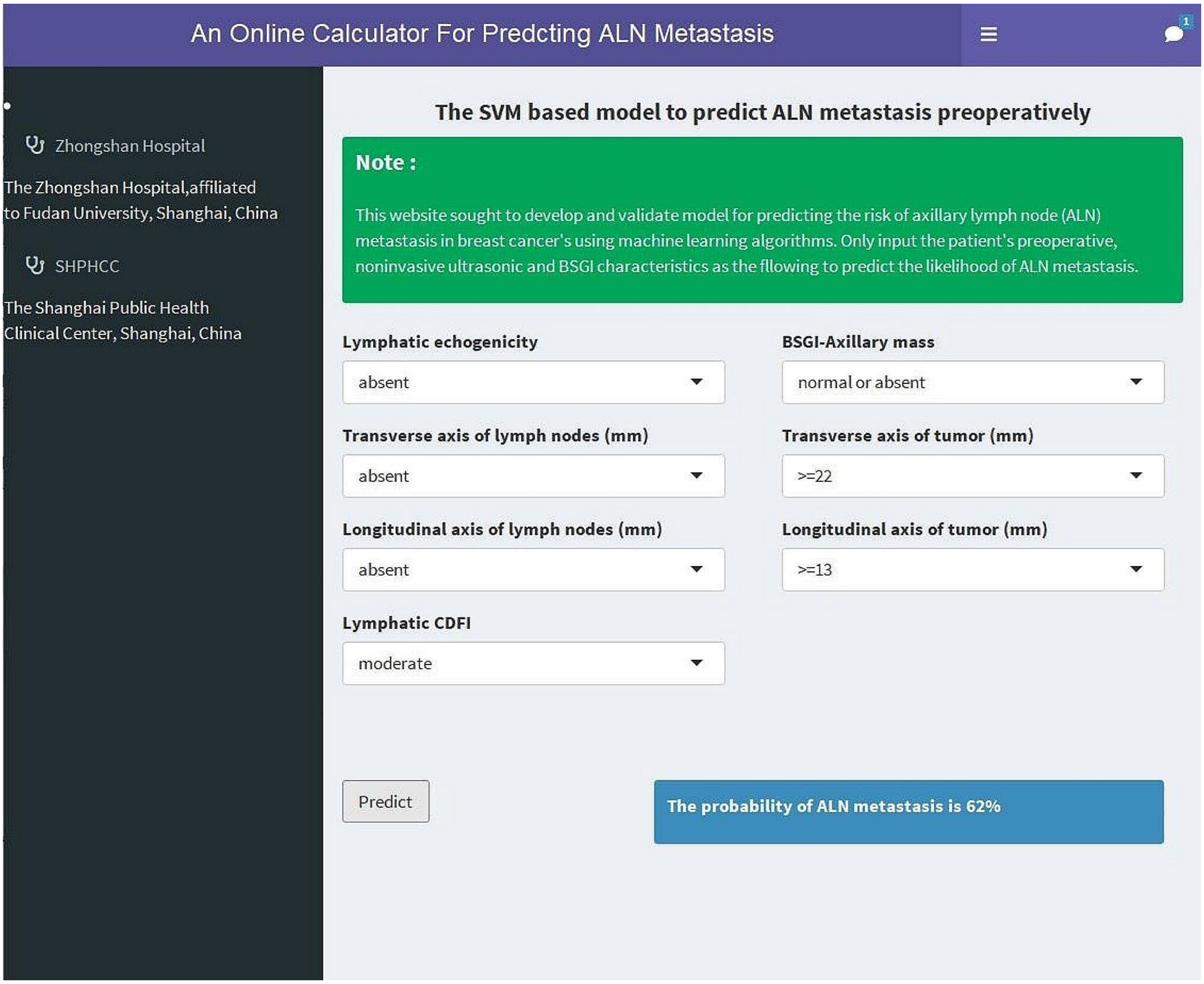

Fig. 5 An online calculator for predcting ALN metastasis. SVM: support vector machine; ALN: axillary lymph node; CDFI: the CDFI grade of lymph node; BSGI: breast-specific gamma imaging

An online calculator was created to facilitate individualized surgical treatment by calculating the risk for each patient of having a positive lymph node (https://wuqian.shinyapps.io/shinybsgi/). For instance, a women with the preoperative US showed a hyperechoic lymph node measuring 9*4 mm, with the CDFI grading absent, the tumour size of 14*10 mm, and the BSGI showed a negative mass in the axilla might be considered to have a approximately 16% risk of ALN metastasis, which implied that axillary surgery could be omitted clinically. Futhermore, the result in ROC analysis showed that the model could benefit from including BSGI features. To the best of our knowledge, no studies have incorporated BSGI features into the prediction model until now, however, the study result is limited and requires much more validation before it can be applied to clinical reasoning.

The advantage of BSGI lies in its combination of the physiological differentiation of the nuclear imaging and the anatomical differentiation of mammography. The semi-quantitative index TNR is traditionally applied in the diagnosis of breast cancer, with a value above 1.65 being considered to be highly suspicious [29], Studies have investigated the association between TNR and clinicopathological characteristics of breast cancer and found a positive correlation with the presence of ALN metastasis [30, 31], which is consistent with our study. In the comparison of the six ML approaches, we found that the tumour TNR was included in the NNET model, but unfortunately the SVM model was the final adoption. Nevertheless, there is no implication that the TNR value has no guidance in clinical practice. For the detection of metastatic ALN, studies showed the sensitivity of BSGI ranges between 67% and 100%, with an average of 81%, and the specificity between 64% and 100% [32]. A positive mass in the axilla indicates the possibility of ALN metastasis more graphically. Although obvious differences

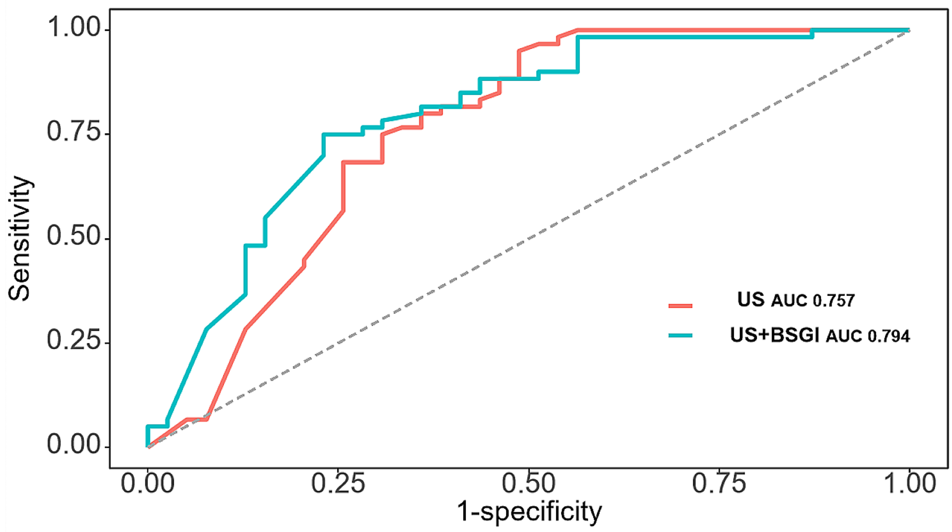

Fig. 6 Evaluation of the model effectiveness with and without the BSGI features by ROC curves. US: Ultrasonography; BSGI: breast-specific gamma imaging; AUC: area under the curve

were shown in the importance of variables among six ML algorithms, axillary mass status held a relatively higher weight in all models.

US is a common preoperative imaging modality for breast cancer, previous studies have suggested that some US features may correlate with the status of ALN, such as cortical thickness of ALN, transverse diameter of ALN, and lymph node hilum status [8, 33]. In our study, both the transverse/longitudinal diameter of the tumour and the lymph node, the echogenicity of the lymph node, and the CDFI grade of the lymph node were all found to be statistically correlated with ALN status. The CDFI grade has been employed in the US to evaluate tumoral angiogenesis, which is a growing trend in breast cancer [34, 35]. Studies also showed that tumour vascularity was correlated with lymph node involvement [36], Chao [37] reported that ALN metastasis had a greater tendency to be present in carcinomas with neovascularisation based on an analyses of 368 patients. However, few researches have investigated the relationship between lymphatic CDFI grade and ALN burden, while our study obtained a positive correlation. Traditionally, hyperechogenicity of a mass are associated with benignity [38] and the same conclusion was reached in this study.

Compared with previous studies attempting to predict the risk of ALN metastases in breast cancer, our work has several strengths. First, few studies have included BSGI-related variables in the model, while a considerable number of studies have compared the specificity and sensitivity of BSGI with MRI and reached favourable conclusions, which confirms the rationality of BSGI as a preoperative modality. The ROC analysis in our study showed that using model with BSGI features provided additional benefit from only ultrasonographic features. Furthermore, all variables included were non-invasive, which might reduce the complications associated with invasive procedures such as SLNB. Finally, we applied ML approach and established an online calculator, which certainly provides the clinical decision making with greater convenience.

However, some limitations of the study were noted. Firstly, despite comparable accuracy to MRI, BSGI remains to be an uncommon modality owing to its high cost and radiation exposure, limiting the promotion of the model. What's more, The relatively low sensitivity of the model reflected the inclusion of fewer patients with ALN metastases in the training data, a limitation that results in showing higher specificity in predicting the absence of ALN metastases. Finally, the model lacks valid external validation given that it was built and validated in the same institution and the nature of a retrospective study all might resulted in selection bias and a slight discrepancy in AUC.

Conclusions

Overall, the trend of de-escalation of axillary surgery is inevitable. In this study, we sought to develop a non-invasive preoperative prediction model to facilitate the subsequent clinical management of patients using ML approach, and for the first time incorporated BSGI-related variables into the model in the hope of provoking subsequent researchers to explore the wider possibilities of BSGI in the management of breast cancer. This study revealed more areas that need future research to validate our findings.

Abbreviations

ALN	axillary lymph node
BSGI	breast specific gamma image

ML	machine learning
ROC	receiver operating characteristic
US	Ultrasonography
MRI	magnetic resonance imaging
DTs	decision trees
ANN	artificial neural networks
SVM	support vector machines
CC	Craniocaudal
MLO	mediolateral oblique
BIRADS	Breast Imaging Reporting and Data System
TNR	tumour-to-normal lesion ratio
ER	estrogen receptor
PR	progesterone receptor
LVI	lymphovascular invasion
SBR	Scarff-Bloom-Richardson
CDFI	color Doppler flow imaging
RI	resistance index
GLM	generalized linear model
RF	random forest
NNET	neural network
GBM	gradient boosting machine
SGB	extreme boosting machine
REF	recursive feature elimination
UOQ	Upper-outer quadrant
LOQ	Lower-outer quadrant
UIQ	Upper-inner quadrant
LIQ	Lower-inner quadrant
PPV	Positive predictive value
NPV	Negative predictive value
AUC	the area under the ROC curve
SLNB	sentinel lymph nodes biopsy
ALND	axillary lymph node dissection

Supplementary Information

The online version contains supplementary material available at https://doi.org/10.1186/s13014-024-02453-2.

Supplementary Material 1

Acknowledgements
Not applicable.

Author contributions
RZ C collected the data and was a major contributor in writing the manuscript; LD analyzed and interpreted the patient data; HZ and HW Z made substantial contributions to the conception; QW designed the work and revised it. All authors reviewed and approved the final manuscript.

Funding
The present study was supported by the Foundation of Zhongshan Hospital (Xiamen), Fudan University (2020ZSXMYS14) and the Natural Science Foundation of Xiamen City (3502Z202373086).

Data availability
The datasets used and/or analysed during the current study are available from the corresponding author on reasonable request.

Declarations

Ethics approval and consent to participate
The ethical approval of this study was granted by ethics committee of Zhongshan Hospital. The need of informed consent was waived by ethics committee of Zhongshan Hospital due to retrospective nature of the study. All experiments were performed with the Declaration of Helsinki.

Consent for publication
Not applicable.

Competing interests
The authors declare no competing interests.

Author details
[1]Department of Neurosurgery, Zhongshan Hospital (Xiamen), Fudan University, Xiamen, Fujian Province 361006, China
[2]Department of General Surgery, Shanghai Public Health Clinical Center, Shanghai 201508, China
[3]Department of General Surgery, Zhongshan Hospital, Fudan University, Shanghai 200032, China
[4]Department of General Surgery, Fudan University Affiliated Huadong Hospital, Shanghai 200040, China

Received: 31 July 2023 / Accepted: 13 May 2024
Published online: 27 May 2024

References

1. Sung H, Ferlay J, Siegel RL, Global Cancer S. 2020: GLOBOCAN estimates of incidence and mortality worldwide for 36 cancers in 185 countries. CA: A Cancer Journal for Clinicians. (2021);71(3):209–49. https://doi.org/10.3322/caac.21660
2. Soares EW, Nagai HM, Bredt LC. Morbidity after conventional dissection of axillary lymph nodes in breast cancer patients. World J Surg Oncol. 2014;12:67. https://doi.org/10.1186/1477-7819-12-67
3. Dinas K, Kalder M, Zepiridis L. Axillary web syndrome: incidence, pathogenesis, and management. Curr Probl Cancer. 2019;43(6):100470. https://doi.org/10.1016/j.currproblcancer.2019.02.002
4. Krag DN, Anderson SJ, Julian TB. Sentinel-lymph-node resection compared with conventional axillary-lymph-node dissection in clinically node-negative patients with breast cancer: overall survival findings from the NSABP B-32 randomised phase 3 trial. Lancet Oncol. 2010;11(10):927–33. https://doi.org/10.1016/S1470-2045(10)70207-2
5. Donker M, van Tienhoven G, Straver ME. Radiotherapy or surgery of the axilla after a positive sentinel node in breast cancer (EORTC 10981–22023 AMAROS): a randomised, multicentre, open-label, phase 3 non-inferiority trial. Lancet Oncol. 2014;15(12):1303–10. https://doi.org/10.1016/S1470-2045(14)70460-7
6. Giuliano AE, Ballman KV, McCall L. Effect of axillary dissection vs no axillary dissection on 10-year overall survival among women with invasive breast cancer and sentinel node metastasis: the ACOSOG Z0011 (Alliance) randomized clinical trial. Jama. 2017;318(10):918–26. https://doi.org/10.1001/jama.2017.11470
7. Bevilacqua JL, Kattan MW, Fey JV. Doctor, what are my chances of having a positive sentinel node? A validated nomogram for risk estimation. J Clin Oncol. 2007;25(24):3670–9. https://doi.org/10.1200/JCO.2006.08.8013
8. Gao Y, Luo Y, Zhao C. Nomogram based on radiomics analysis of primary breast cancer ultrasound images: prediction of axillary lymph node tumor burden in patients. Eur Radiol. 2021;31(2):928–37. https://doi.org/10.1007/s00330-020-07181-1
9. Huppe AI, Mehta AK, Brem RF. Molecular breast imaging: a comprehensive review. Semin Ultrasound CT MR. 2018;39(1):60–9. https://doi.org/10.1053/j.sult.2017.10.001
10. Kolb TM, Lichy J, Newhouse JH. Comparison of the performance of screening mammography, physical examination, and breast US and evaluation of factors that influence them: an analysis of 27,825 patient evaluations. Radiology. 2002;225(1):165–75. https://doi.org/10.1148/radiol.2251011667
11. Rhodes DJ, Hruska CB, Conners AL. Journal club: molecular breast imaging at reduced radiation dose for supplemental screening in mammographically dense breasts. AJR Am J Roentgenol. 2015;204(2):241–51. https://doi.org/10.2214/AJR.14.13357
12. Rechtman LR, Lenihan MJ, Lieberman JH. Breast-specific gamma imaging for the detection of breast cancer in dense versus nondense breasts. AJR Am J Roentgenol. 2014;202(2):293–8. https://doi.org/10.2214/AJR.13.11585
13. Villanueva-Meyer J, Leonard MJ, Briscoe E. Mammoscintigraphy with technetium-99m-sestamibi in suspected breast cancer. J Nucl Med. 1996;37(6):926–30.
14. Werner J, Rapelyea JA, Yost KG. Quantification of radio-tracer uptake in axillary lymph nodes using breast specific gamma imaging (BSGI): benign radio-tracer extravasation versus uptake secondary to breast cancer. Breast J. 2009;15(6):579–82. https://doi.org/10.1111/j.1524-4741.2009.00834.x

15. Stojadinovic A, Nissan A, Eberhardt J. Development of a bayesian belief network model for personalized prognostic risk assessment in colon carcinomatosis. Am Surg. 2011;77(2):221–30.
16. Lee JH, Ha EJ, Kim D. Application of deep learning to the diagnosis of cervical lymph node metastasis from thyroid cancer with CT: external validation and clinical utility for resident training. Eur Radiol. 2020;30(6):3066–72. https://doi.org/10.1007/s00330-019-06652-4
17. Goldsmith SJ, Parsons W, Guiberteau MJ. SNM practice guideline for breast scintigraphy with breast-specific gamma-cameras 1.0. J Nucl Med Technol. 2010;38(4):219–24. https://doi.org/10.2967/jnmt.110.082271
18. Adler DD, Carson PL, Rubin JM. Doppler ultrasound color flow imaging in the study of breast cancer: preliminary findings. Ultrasound Med Biol. 1990;16(6):553–9. https://doi.org/10.1016/0301-5629(90)90020-d
19. Meretoja TJ, Leidenius MH, Heikkilä PS. International Multicenter tool to predict the risk of nonsentinel node metastases in breast cancer. J Natl Cancer Inst. 2012;104(24):1888–96. https://doi.org/10.1093/jnci/djs455
20. Al-Hilli Z, Hieken TJ, Boughey JC. Axillary Ultrasound in the management of the newly diagnosed breast Cancer patient. Breast J. 2015;21(6):634–41. https://doi.org/10.1111/tbj.12497
21. Harrell FJ, Lee KL, Mark DB. Multivariable prognostic models: issues in developing models, evaluating assumptions and adequacy, and measuring and reducing errors. Stat Med. 1996;15(4):361–87. https://doi.org/10.1002/(SICI)1097-0258(19960229)15:4%3C361::AID-SIM168%3E3.0.CO;2-4
22. Buxton RT, McKenna MF, Clapp M. Efficacy of extracting indices from large-scale acoustic recordings to monitor biodiversity. Conserv Biol. 2018;32(5):1174–84. https://doi.org/10.1111/cobi.13119
23. Huang ML, Hung YH, Lee WM. SVM-RFE based feature selection and Taguchi parameters optimization for multiclass SVM classifier. Scientific World Journal. (2014);2014:795624. https://doi.org/10.1155/2014/795624
24. Ngiam KY, Khor IW. Big data and machine learning algorithms for healthcare delivery. Lancet Oncol. 2019;20(5):e262–73. https://doi.org/10.1016/S1470-2045(19)30149-4
25. Van Calster B, Wynants L, Verbeek J. Reporting and interpreting decision curve analysis: a guide for investigators. Eur Urol. 2018;74(6):796–804. https://doi.org/10.1016/j.eururo.2018.08.038
26. Mansel RE, Fallowfield L, Kissin M. Randomized multicenter trial of sentinel node biopsy versus standard axillary treatment in operable breast cancer: the ALMANAC Trial. J Natl Cancer Inst. 2006;98(9):599–609. https://doi.org/10.1093/jnci/djj158
27. Zhu J, Zheng J, Li L. Application of machine learning algorithms to predict central lymph node metastasis in T1-T2, non-invasive, and clinically node negative papillary thyroid carcinoma. Front Med (Lausanne). 2021;8:635771.
28. Wu Y, Rao K, Liu J. Machine learning algorithms for the prediction of central lymph node metastasis in patients with papillary thyroid cancer. Front Endocrinol (Lausanne). 2020;11:577537.
29. Liu H, Zhan H, Sun D. Comparison of BSGI, MRI, mammography, and ultrasound for the diagnosis of breast lesions and their correlations with specific molecular subtypes in Chinese women. BMC Med Imaging. 2020;20(1):98. https://doi.org/10.1186/s12880-020-00497-w
30. Cwikla JB, Buscombe JR, Kolasinska AD. Correlation between uptake of Tc-99m sestaMIBI and prognostic factors of breast cancer. Anticancer Res. 1999;19(3B):2299–304.
31. Bonazzi G, Cistaro A, Bellò M. Breast cancer cellular proliferation indexes and 99mTc-sesta Mibi capture: what correlation? J Exp Clin Cancer Res. 2001;20(1):91–4.
32. Lumachi F, Ferretti G, Povolato M. Usefulness of 99m-Tc-sestamibi scintimammography in suspected breast cancer and in axillary lymph node metastases detection. Eur J Surg Oncol. 2001;27(3):256–9. https://doi.org/10.1053/ejso.2000.1096
33. Qiu SQ, Zeng HC, Zhang F. A nomogram to predict the probability of axillary lymph node metastasis in early breast cancer patients with positive axillary ultrasound. Sci Rep. 2016;6:21196. https://doi.org/10.1038/srep21196
34. Sehgal CM, Weinstein SP, Arger PH. A review of breast ultrasound. J Mammary Gland Biol Neoplasia. 2006;11(2):113–23. https://doi.org/10.1007/s10911-006-9018-0
35. Khosravi SP, Soria LA, Pérez MG. Tumoral angiogenesis and breast cancer. Clin Transl Oncol. 2009;11(3):138–42. https://doi.org/10.1007/s12094-009-0329-7
36. Shen ZY, Hu B, Wu MF. Correlation between blood flow signal of color flow imaging and nottingham prognostic index in patients with breast carcinoma. Breast Care (Basel). 2012;7(2):126–30. https://doi.org/10.1159/000337766
37. Chao TC, Luo YF, Chen SC. Color Doppler ultrasound in breast carcinomas: relationship with hormone receptors, DNA ploidy, S-phase fraction, and histopathology. Ultrasound Med Biol. 2001;27(3):351–5. https://doi.org/10.1016/s0301-5629(00)00345-8
38. Stavros AT, Thickman D, Rapp CL. Solid breast nodules: use of sonography to distinguish between benign and malignant lesions. Radiology. 1995;196(1):123–34. https://doi.org/10.1148/radiology.196.1.7784555

Publisher's Note